
Laser Assisted Photoelectric Effect from Metal Surfaces

Jan Conrad Baggesen

...

Progress report

Lundbeck Foundation Theoretical Center for Quantum System Research
Department of Physics and Astronomy
Aarhus University
June 18, 2009.



Contents

Preface	ii
Notation	ii
Acknowledgements	ii
1 Introduction	1
2 Laser Assisted Photoelectric Effect	2
2.1 Modelling Laser Assisted Photoemission	3
2.2 xuv Pulses much Shorter than the Laser Period	5
2.3 xuv Pulses longer than the Optical Period	7
3 Solid State Models	9
3.1 The Jellium Model	9
3.1.1 Sidebands in Conduction Band Spectra	11
3.2 Core Level States	13
3.3 Delay of Core Electrons Relative to Conduction Band	14
4 Secondary Electrons	17
4.1 Single-Scattering Theory	17
4.2 Cascade Theory	20
4.3 Probability for Escaping Through the Surface	22
4.4 Application to Tungsten Experiment	23
5 Conclusions and Outlook	27
5.1 Transport Theory	27
5.2 Gaussian States	28
Bibliography	30



Preface

This progress report contains a summary of the work carried out during part A of my PhD studies at the Lundbeck Foundation Theoretical Center for Quantum System Research, Department of Physics and Astronomy, Aarhus University.

This work has resulted in one published paper[1] on time-resolved measurements using the laser assisted photoelectric effect from the conduction band of a metal and another that is in progress[2] on secondary electrons in attosecond spectroscopy from metal surfaces. In the report, the chapters cover first general theory of the laser assisted photoelectric effect, then solid state models, needed to describe the metal surface and finally theory for the secondary electrons emitted.

Notation

Atomic units, $e = m_e = \hbar = a_0 = 1$, are used throughout this report, unless otherwise stated.

Acknowledgements

I would like to thank my supervisor Lars Bojer Madsen for introducing me to this brand new and very exciting field of physics and for his inspiring supervision. I would also like to thank Lisbeth Munksgaard Nielsen and Anne Ivalu Sander Holm for proofreading this manuscript and suggesting many improvements.

Introduction

In recent years, tremendous progress has been made within the field of short laser pulses. Now, it is possible to make phase-stabilized few cycle laser pulses and to use these to make attosecond pulses, short enough to follow electron dynamics within atoms and molecules. This opens a lot of new opportunities in the field of ultrafast spectroscopy.

When electrons are exposed to a very intense laser field, electrons may be driven away from the nucleus and back to recombine. The recombination results in the emission of a photon with potentially very high energy, called high-order harmonics. This way laser pulses with central frequency of around 100 eV, may be formed from a light pulse with wavelength around 800 nm. If the infrared laser pulse contains only a very few optical periods, a single field maximum may be dominant and the result is a single pulse with a duration of only a few hundred attoseconds[3]. These pairs of pulses are ideal for time-resolved pump-probe spectroscopy. Since the high energy pulse is formed from the very short infrared pulse, the relative delay between the two pulses is well known and even controllable.

Very recently, experimental and theoretical interest has started to form about ultrafast spectroscopy from metal surfaces. Using these tools from atomic and molecular physics it is possible to study ultrafast processes in and on metal surfaces and to use the very high electron and atom density of solids to characterize the laser pulses[4] and the attosecond pulses. It has been used to measure a delay of only 110 attoseconds between electrons released from the conduction band of tungsten and electrons released the core 4f level[5] and to measure the Auger lifetime of a xenon atom adsorbed on a platinum surface[6].

This report is dedicated to the theory needed to model the laser assisted photoelectric effect from metal surfaces and to use this for time-resolved measurements. The two experiments [5] and [6] will repeatedly be brought up as motivation for the theory and for comparison.

Laser Assisted Photoelectric Effect

In laser assisted photoelectric effect (LAPE) experiments, two pulses are incident on a target, in this case a metal surface. One is the ionizing pulse, a weak, very short pulse with wavelengths in the extreme ultra-violet (xuv). The assisting laser pulse is much more intense and has a central wavelength in the near infrared, typically around 800 nm which is produced by TI:Sapphire lasers. The two laser pulses allow time-resolved measurements, by varying the relative delay between them. The xuv pulse is produced by using part of the infrared pulse for high harmonic generation. This allows for a very precise timing of the delay between the two. After ionization, the liberated electron interacts with the strong assisting pulse, resulting in a spectrum with a signature of the overlap of the two pulses. Two different regimes are of particular interest; i) when the xuv pulse is much shorter than the optical period of the laser and ii) when the xuv pulse is comparable to the optical period or longer.

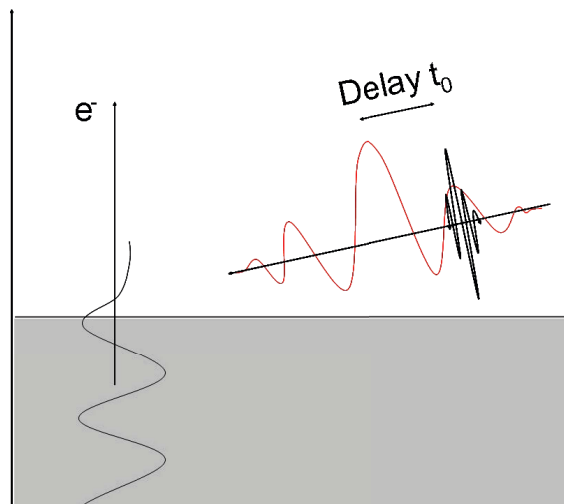


Figure 2.1 | Diagrammatic illustration of the laser assisted photoelectric effect. Two pulses with variable delay, t_0 , are incident on a metal surface, resulting in emission of electrons with signatures of the overlap of the pulses.

In the limit of long pulses with a definite frequency, this gives rise to a central main peak in the photoelectron energy spectrum and a series of sidebands equally spaced an integer number of infrared photon-energies to each side of the main peak[7]. This corresponds to the electron exchanging an integer number of photons with the field. The magnitude of these sidebands is proportional to the instantaneous laser intensity at the time of electron emission. From metal surfaces, the laser assisted photoelectric effect was first seen in 2006 by Miaja-Avila et al.[8]. These sidebands may be used for time-resolved measurements. One use of this is to measure the lifetime of xenon $4d^{-1}$ core level directly in the time domain[6], for an xenon atom adsorbed on a platinum surface. This Auger lifetime is only 7 fs, showing the very fine temporal resolution. The atomic Auger lifetime, τ is previously measured in the energy domain, using $\tau\Gamma \sim \hbar/2$, where Γ is the natural line width of the transition. This requires that you can measure the natural line width of the Auger peak, which is very difficult for an adsorbed atom, because of the broad range of phenomena happening on a metal surface. The technique used in [6] is to find the magnitude of the sidebands as a function of delay, for both the direct electrons and for the Auger electrons. The temporal shift of the peak gives the lifetime of the transition. The theory of these sidebands formed from short laser pulses will be presented later.

High-order harmonic generation can be used to make pulses with sub-fs duration[9]. In the limit of xuv pulses much shorter than the optical period of the assisting laser field, the approximation is that the electrons are all liberated at the same time, t_0 , when the electric field of the laser pulse has a definite value $\mathcal{E}(t_0)$. In a classical model, the electrons are then driven by the electric field, gaining an amount of momentum $\Delta p = -\int_{t_0}^{\infty} dt \mathcal{E}(t) = A(t_0)$. In this way, measuring the change in energy $\Delta E \sim p\Delta p$, the vector potential may be mapped directly, in the limit where $\Delta p \ll p$ [10]. This experiment is very delicate. It requires a phase stabilized laser pulse and it requires an xuv pulse no longer than a few hundred attoseconds (1 asec = $10^{-18}s$). The advantage is, however, that the temporal precision is determined by the laser period, allowing direct measurements of only a few hundred attoseconds. The prime example is that a temporal delay between core $4f$ -electrons and conduction band electrons of only 110 asec has been measured from a tungsten surface[5]. The spectrum produced in the experiment is shown in Fig. 2.2.

2.1 Modelling Laser Assisted Photoemission

Because the main focus is on understanding the dynamical processes involved, it is essential to develop a model that is able to treat the short laser pulses correctly. The price we have to pay for being able to treat the full temporal dependence of the problem is that we cannot cover the complexity of the metal and have to settle for simple metal models. The models used to treat photoemission by short pulses are inspired by similar models used to treat photoionization of atoms and molecules with short laser pulses. To get the differential probability for promoting an electron from a bound state i to a continuum state with momentum \vec{k}_f , we must take the norm-square of the transition matrix element, T_{fi} defined by

$$T_{fi} = -i \int dt \langle \Psi_f(t) | V(t) | \Psi_i(t) \rangle. \quad (2.1)$$

For atoms and small molecules, the distance between different energy levels is usually so big, that only one ionization channel makes a significant contribution. This is, however, not the case for metals. When many energy levels contribute, the photoemission signal in

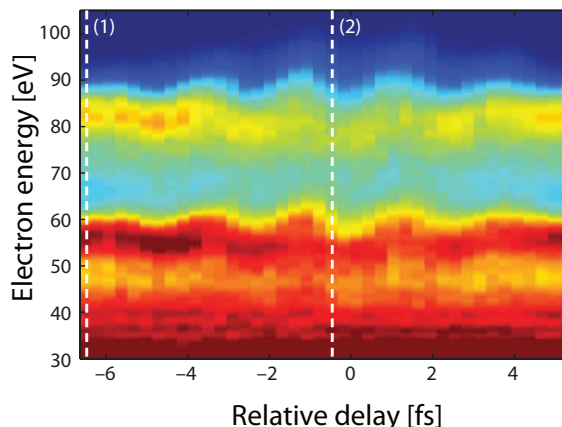


Figure 2.2 | The experimental spectrum from [5]. Along the horizontal axis is the relative delay between the attosecond xuv pulse and the infrared laser pulse in fs. Along the vertical axis is the photoelectron energy in eV. The topmost peak around 83 eV is electrons emitted from the conduction band, while the peak around 56 eV is electrons emitted from localized 4f-states. Detailed analysis reveals that the streaking of the 4f-electrons is delayed 110 asec relating to the conduction band electrons.

the final channel \vec{k}_f is given by the incoherent sum over the contribution from all of the occupied states in the metal

$$P(\vec{k}_f) = 2 \sum_i |T_{fi}|^2, \quad (2.2)$$

where i runs through all occupied states, that is all states with energy below the Fermi energy. The first point to explore is how far one can actually get, without saying much about the initial states of the metal. This is a way to explore very general features of the laser assisted photoelectric effect.

In order to determine T_{fi} , the first thing needed is the interaction. The light-matter interaction is modelled in the length gauge and in the dipole approximation:

$$V(t) = \vec{r} \cdot \vec{\mathcal{E}}(t) = \vec{r} \cdot (\vec{\mathcal{E}}_X(t) + \vec{\mathcal{E}}_L(t)), \quad (2.3)$$

where $\vec{\mathcal{E}}_X(t)$ and $\vec{\mathcal{E}}_L(t)$ is the electric field vectors of the xuv pulse and the laser pulse respectively. The two terms may be identified as ionization due to xuv pulse and above threshold ionization(ATI) due to the infrared pulse. Since the ATI contribution falls off rapidly with increasing electron energy, it is negligible in the energy region of interest. Thus only the xuv interaction is included in the calculations and the main focus is on electrons emitted upon one xuv photon absorption.

The dipole approximation may seem devious, as the length scale of a metal is much larger than the wavelength of the radiation. The pulse, however, has a finite penetration depth and the electrons have a finite inelastic mean free path within the metal, both of which are much shorter than the wavelength of the xuv pulse. This justifies the use of the dipole approximation.

The final state is excited high above the conduction band and resembles a free electron state very closely. The wavefunction of a free electron in an electromagnetic field is known as a Volkov wave. It is given by

$$\Psi_f(\vec{r}, t) = \Psi_k^V(\vec{r}, t) = \frac{1}{(2\pi)^{3/2}} \exp \left[i(\vec{k} + \vec{A}(t)) \cdot \vec{r} - \frac{i}{2} \int^t dt' (\vec{k} + \vec{A}(t'))^2 \right], \quad (2.4)$$

where

$$\vec{A}(t) = - \int^t dt' \vec{\mathcal{E}}(t') \quad (2.5)$$

is the vector potential at time t . Since the xuv pulse is very weak compared to the infrared pulse, we may ignore the xuv pulse in Eq. (2.4). The wavefunction presented in Eq. (2.4) is the usual free electron wavefunction, with momentum $\vec{k} + \vec{A}(t)$ replacing the asymptotic momentum \vec{k} .

Even if the physically relevant field is the \mathcal{E} -field in the length gauge, it is often easier to model the vector potential first and then derive the electric field as $\vec{\mathcal{E}} = -\frac{d\vec{A}(t)}{dt}$. The requirement is that the vector potential must vanish at $t \rightarrow \infty$, to avoid a DC component in the electric field, which is not allowed for a propagating pulse. The laser pulses may be modelled as an oscillating field with a Gaussian envelope, as

$$\vec{A}_i(t) = \vec{\epsilon} A_{0,i} \exp\left(-2 \ln(2) \frac{(t - t_0)^2}{\tau_i^2}\right) \cos(\omega_i t + \phi), \quad (2.6)$$

where i may be either X for the xuv pulse or L for the infrared laser pulse, $\vec{\epsilon}$ is the polarization, $A_{0,i}$ is the peak amplitude, τ_i is the full width at half maximum (FWHM) of the intensity of the pulse, ω_i is the central frequency and ϕ is the carrier envelope phase. For long pulses, the carrier envelope phase is usually unimportant, but once the duration of the pulse is only a few times the period of the oscillation it becomes important, especially when considering non-linear effects. In atomic units, the amplitude for the vector potential relates to the experimentally preferred peak intensity in W/cm^2 , through

$$\mathcal{E}_{0,i} = \sqrt{\frac{I}{3.51 \cdot 10^{16} \text{W}/\text{cm}^2}}, \quad (2.7)$$

and $A_{0,i} = \frac{\mathcal{E}_{0,i}}{\omega_i}$.

2.2 xuv Pulses much Shorter than the Laser Period

In the limit where the xuv pulse is much shorter than the optical period of the assisting laser field, the value of the vector potential is essentially constant while the xuv pulse is on. This is the case, when using some of the shortest attosecond pulses, with duration around 100-300 asec and 800 nm infrared pulses with an optical period just above 2 fs. In this limit, the temporal integral in Eq. (2.1) may be performed analytically, by holding the value of the laser field constant at the value at the center of the xuv pulse, t_0 .

$$\begin{aligned} T_{fi} &= -i \int dt \langle \Psi_f(t) | \vec{r} \cdot \vec{\mathcal{E}}_X(t) | \Psi_i(t) \rangle \\ &= -i \langle \psi_{\vec{k} + A_L(t_0)}(\vec{r}) | \vec{\epsilon}_X \cdot \vec{r} | \psi_i(\vec{r}) \rangle \int dt \exp\left[-\frac{i}{2} \int^t dt' (\vec{k} + \vec{A}_L(t'))^2\right] \left(-\frac{dA_X}{dt}\right) e^{-iE_i t}, \end{aligned} \quad (2.8)$$

where $\psi_{\vec{k}}$ is the free electron wavefunction with momentum \vec{k} , that is $\psi_{\vec{k}}(\vec{r}) = (2\pi)^{-3/2} e^{i\vec{k} \cdot \vec{r}}$. Assuming that the laser potential is constant during the attosecond pulse, the integral in the exponential may be approximated as

$$\int^t dt' (\vec{k} + \vec{A}_L(t'))^2 = \int^{t_0} dt' (\vec{k} + \vec{A}_L(t'))^2 + (\vec{k} + \vec{A}_L(t_0))^2 (t - t_0), \quad (2.9)$$

where the first part is now a phasefactor, independent of t that may be taken outside the time integral. Performing partial integration on the integral in Eq. (2.8) to gives

$$\begin{aligned}
 T_{fi} &= -i \exp \left[-\frac{i}{2} \int^{t_0} dt' (\vec{k} + \vec{A}_L(t'))^2 \right] \langle \psi_{k+A_L(t_0)}(\vec{r}) | \vec{\epsilon}_X \cdot \vec{r} | \psi_i(\vec{r}) \rangle \\
 &\times \int dt A_X(t) i [(\vec{k} + \vec{A}_L(t_0))^2 / 2 - E_i] \exp \left[i \{ (\vec{k} + \vec{A}_L(t_0))^2 / 2 - E_i \} t \right]. \quad (2.10)
 \end{aligned}$$

The boundary terms in the partial integration vanishes, since $A_X(t)$ goes to zero. To shorten the notation, $\Delta E(t_0) = [(\vec{k} + \vec{A}(t_0))^2 / 2 - E_i]$ is introduced. This gives the difference in energy between the initial state of the bound electron and the energy that is needed for the electron to end up with an asymptotic momentum \vec{k} after having propagated in the laser field.

Since the attosecond pulse is rather weak, the probability of driving the electron back and forth is negligible and it is safe to include only the energy conserving part of the interaction, corresponding to the replacing $\cos(\omega_X t + \phi) \rightarrow \frac{1}{2} e^{-i(\omega_X t + \phi)}$ in Eq. (2.6). This is known as the rotating wave approximation. In the end, the time integration is a Fourier transform of the Gaussian envelope function, that may be calculated analytically

$$\begin{aligned}
 T_{fi} &= \Delta E(t_0) \exp \left[-\frac{i}{2} \int^{t_0} dt' (\vec{k} + \vec{A}(t'))^2 - i\phi \right] \langle \psi_{k+A(t_0)}(\vec{r}) | \vec{\epsilon}_X \cdot \vec{r} | \psi_i(\vec{r}) \rangle \\
 &\times \int dt A_{0,X} \exp \left(-2 \ln(2) \frac{(t - t_0)^2}{\tau_i^2} \right) e^{-i(\omega_X t - \Delta E(t_0)t)} \quad (2.11)
 \end{aligned}$$

$$\begin{aligned}
 &= \Delta E(t_0) \exp \left[-\frac{i}{2} \int^{t_0} dt' (\vec{k} + \vec{A}(t'))^2 - i\phi \right] \langle \psi_{k+A(t_0)}(\vec{r}) | \vec{\epsilon}_X \cdot \vec{r} | \psi_i(\vec{r}) \rangle \\
 &\times \sqrt{\frac{\pi}{8 \ln(2)}} A_{0,X} \tau_X \exp \left[-\frac{\tau_X^2 (\omega_X - \Delta E(t_0))^2}{8 \ln 2} \right] \quad (2.12)
 \end{aligned}$$

The interesting part is of course the norm square of the T -matrix elements, which are used in Eq. (2.2). Taking the norm square of Eq. (2.12) gives

$$|T_{fi}|^2 = \frac{\pi}{8 \ln 2} A_{0,X}^2 \tau_X^2 \Delta E(t_0)^2 \exp \left[-\frac{\tau_X^2 (\omega_X - \Delta E(t_0))^2}{4 \ln 2} \right] |\langle \psi_{k+A(t_0)}(\vec{r}) | \vec{\epsilon}_X \cdot \vec{r} | \psi_i(\vec{r}) \rangle|^2. \quad (2.13)$$

If one is able to evaluate the time independent overlap between the initial state and the free electron final state, then it gives an analytical description of the electron spectrum as a function of the variable time delay, t_0 .

Looking at this expression, the signal is a peak of photoelectrons with energy centered around $\omega_X - \Delta E(t_0) = 0$, which is exactly the energy expected from a classical analysis of ionization followed by the propagation of a free electron in an electric field. When the assisting laser pulse is short, mapping out the energy spectrum as a function of delay gives a mapping of the vector potential of the assisting laser pulse, that is a signature of the time of emission.

Below, the free electron model is presented in Sec. 3.1. Here the results are used in advance to test validity of the analytic approach above. In the experiment in Ref. [5], an attosecond pulse with a FWHM of 300 asec and a central frequency of $\hbar\omega_X = 91$ eV is used as the ionizing pulse and an intense laser pulse, with a central frequency of 750 nm is the assisting laser pulse. In Fig. 2.3 the photoelectron spectrum as a function of the variable delay is calculated. As seen, the results are almost identical, the major difference being

only the density of points. Since the right hand side is calculated using full numerical integration of the time dependence, it is much more computationally heavy and it is not possible to get the same kind of resolution as in the left hand side. In the calculation, the intensity of the assisting pulse is taken to be $2 \cdot 10^{12}$ W/cm² and the polarization are taken to be normal to the surface.

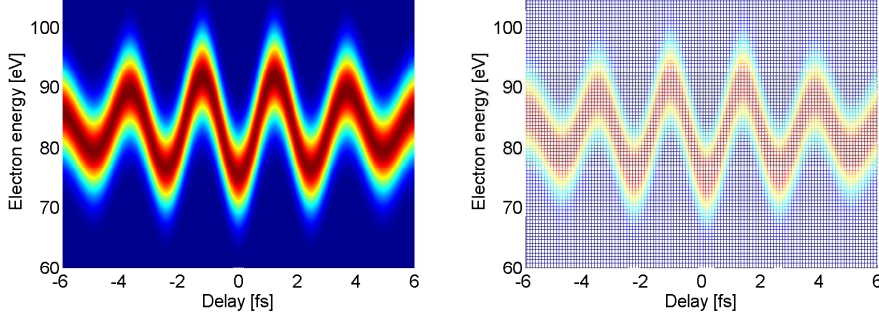


Figure 2.3 | Photoelectron spectra as function of the temporal delay between the two pulses. The left hand side is calculated by the analytical approach, Eq. (2.12), while the right hand side is calculated by numerical integration of Eq. (2.1). The initial states are the free electron states from the jellium model.

2.3 xuv Pulses longer than the Optical Period

When the xuv pulse is longer than the optical period of the assisting laser field, the above approximation is of course not valid and the temporal integral has to be performed numerically. In the opposite limit, when both the ionizing and the assisting laser field are very long, the problem may be solved analytically[7]. In this case it is found that the ratio of the sidebands to the primary peak are given as

$$P_n = J_n^2\left(\frac{\vec{k} \cdot \vec{\mathcal{E}}_{0,L}}{\omega_L^2}, \frac{U_p}{2\omega_L}\right), \quad (2.14)$$

where $J_n(x, y)$ is the generalized Bessel function of integer order, n , \vec{k} is the momentum of the electron in the main peak and $U_p = \mathcal{E}_L^2/4\omega_L^2$ is the ponderomotive potential. The ponderomotive potential is the classical quiver energy of a free electron in an oscillating electric field. The primary interest is with the first sideband, which is the strongest for reasonable laser intensities. As long as the assisting field is not too big, the ponderomotive potential is quite small and the second argument is vanishing. When this is the case, the ratio of the first sideband to the central peak is given as

$$P_1 \sim J_1^2\left(\frac{\vec{k} \cdot \vec{\mathcal{E}}_0}{\omega_L^2}, 0\right) = J_1^2\left(\frac{\vec{k} \cdot \vec{\mathcal{E}}_0}{\omega_L^2}\right), \quad (2.15)$$

where $J_1(x)$ is the ordinary Bessel function of the order 1.

This analysis is expected to be valid when both the laser pulse and the xuv pulse is much longer than the optical period of the laser pulse. One question to address is how long these pulses must be, before we no longer see these sidebands and cannot use them as signatures for time resolved measurements. As seen above, in the limit of very short

xuv pulses, there are no sidebands. This may be understood, as the xuv pulse gets so short and hence so spectrally wide that the sidebands are within the spectral width of the pulse and cannot be resolved. When the aim of this exercise is to be able to perform ultrafast spectroscopy, the key is of course the temporal resolution. In this case, the relative magnitude of the sidebands is dependent on the intensity of the assisting pulse and the temporal resolution is determined by the duration of the pulse. This will be addressed in Sec. 3.1.1.

Solid State Models

In the previous chapter the general theory for LAPE was presented. In order to apply this to metal surfaces, what is left is to calculate the dipole matrix elements, entering in Eq. (2.1). To find these, what is now needed is a model giving the initial states within the metal. A model for the conduction band electrons in terms of free electrons located in half-space is presented. This model is known as the jellium or the Sommerfeld model for metals. To describe core electrons within the metal, we use Bloch waves of atomic levels. The core electrons are localized quite close to the nucleus and is hence a lot less affected by the neighbouring atoms. The atomic levels are therefore a good approximation. Both of these models are presented below.

3.1 The Jellium Model

The jellium model is a very simple model for a metal surface[11]. The Hamiltonian describing the system is a step function in z -direction

$$H = \frac{p^2}{2} + \Theta(z)V_0, \quad (3.1)$$

where $\Theta(z)$ is the Heaviside step function, 0 for $z < 0$ and 1 for $z > 0$ and V_0 is the size of the step. V_0 is the amount of energy needed to release an electron from the bottom of the conduction band, given by the sum $V_0 = E_F + \phi$, where E_F is the Fermi energy, the energy of the weakest bound electron and ϕ is the workfunction, the energy needed to release the weakest bound electron into vacuum. An actual metal is of course a lot more complicated, but since all the nuclei are screened by the electrons, the jellium potential is a fair effective potential for the electrons. The electronic states are found by the Aufbau principle, filling all eigenstates with energy below E_F .

The Hamiltonian is separable in Cartesian coordinates, and the solution to the x and y part is seen to be the free electron wave function

$$\psi(x, y, z) = \psi_{\parallel}(x, y)\psi_{\perp}(z) = \frac{1}{2\pi}e^{i\vec{k}_{\parallel}\cdot\vec{r}_{\parallel}}\psi_{\perp}(z), \quad (3.2)$$

where ψ_{\parallel} and ψ_{\perp} is the wavefunction parallel and perpendicular to the metal surface respectively. The problem of finding the full eigenstates has now been reduced to the one-

dimensional problem of a step function. The energy of the eigenstate ψ is $E = E_{||} + E_{\perp} = \frac{k_{||}^2}{2} + E_z$.

To find the bound eigenstates of the jellium Hamiltonian, it is seen that the potential is constant for both $z < 0$ and $z > 0$. Looking at $E_z < V_0$, the functional form of the solution in the two regions is

$$Ae^{ik_z z} + Be^{-ik_z z} \quad z < 0 \quad (3.3)$$

$$Ce^{-\gamma z} \quad z > 0, \quad (3.4)$$

where the exponentially growing part in $z > 0$ has been discarded. Here $E_z = \frac{k_z^2}{2} = V_0 - \gamma^2/2$. What is left in order to find the stationary states is to match the two solutions in $z = 0$. Both the wavefunction and the first derivative of the wavefunction must be continuous. Enforcing both these requirements gives the solutions

$$\psi_{\perp}(z) = A \left(e^{ik_z z} + \frac{k_z - i\gamma}{k_z + i\gamma} e^{-ik_z z} \right) \Theta(-z) + A \frac{2k_z}{k_z + i\gamma} e^{-\gamma z} \Theta(z). \quad (3.5)$$

Normalization is chosen as $A = \frac{1}{\sqrt{2\pi}}$, similar to the normalization of the free electron states. With this choice of normalization, the bound state wavefunctions satisfy that

$$\langle \psi_{k'}(z) | \psi_k(z) \rangle = \delta(k - k'), \quad (3.6)$$

and the three dimensional wavefunctions satisfy a similar relation with the three dimensional delta function. Along with the choice of normalizations comes a density of states, in three dimensional k -space is $\rho(\vec{k})d^3k = \frac{V}{8\pi^3}d^3k$ [11]. The density of states in energy-space is then given by

$$\rho(E)dE = \frac{3n}{2E_F} \sqrt{\frac{E}{E_F}}, \quad (3.7)$$

where n is the density of conduction band electrons (number per volume) and E_F is the Fermi energy, the energy of the highest occupied state.

The free electron model is quite good at describing the conduction band of simple metals, but unfortunately, not all metals are free electron like. Tungsten, which is the metal used in the streaking experiment[5], is unfortunately not very free electron like. The density of states within the conduction band, as calculated in[12] shows a lot of structure and does not follow the square root dependence predicted by free electron theory. The free electron model is however applied due to the simplicity and the fact that many of the time-resolution issues of interest are not greatly dependent on the material model. When the laser fields are both at grazing incidence, with the polarization vector orthogonal to the surface, the dipole matrix elements may be calculated analytically.

When calculating photoemission spectra, it is necessary to include the finite mean free path within the metal. After an electron has been excited to an unbound state, it will propagate, on average, only the mean free path before being scattered. The dominating part of this scattering is electron-electron scattering as will be discussed in the next chapter. The inelastic mean free path for electrons with a kinetic energy around 50-100 eV within the metal is of the order of only 5 Å[13], shorter than the penetration depth of the xuv field, even at grazing incidence and comparable to the inter-atomic spacing. This implies that only the outermost electrons may be emitted directly. A simple way to incorporate this limited mean free path, λ , is to let the free electron wavefunction fall

of exponentially within the metal, $\psi^V \rightarrow \psi^V e^{z/2\lambda} = \psi^V e^{\kappa z}$, where $\kappa = (2\lambda)^{-1}$ and the 2 ensures that the norm-square of the wavefunction is damped with the mean free path as damping parameter. The spatial dependence of ψ^V is like a free electron with the momentum shifted by the vector potential

$$\psi_{k_f}^V(\vec{r}) = \frac{1}{(2\pi)^{3/2}} e^{i(\vec{k}_f + \vec{A}(t)) \cdot \vec{r}} = \psi_{k_f + A(t)}(\vec{r}) \quad (3.8)$$

Calculating the dipole matrix element, neglecting the purely time-dependent phases, one gets

$$\begin{aligned} \langle \psi_{k_f + A(t)}(\vec{r}) | z | \psi_{k_i}(\vec{r}) \rangle &= \frac{\delta(\vec{k}_{f,\parallel} - \vec{k}_{i,\parallel})}{\sqrt{2\pi}} \int dz \exp[-i(k_{f,z} + A(t) - i\kappa)z] z \psi_{\perp}(z) \\ &= \frac{\delta(\vec{k}_{f,\parallel} - \vec{k}_{i,\parallel})}{2\pi} \left\{ \int_0^{\infty} dz z e^{-i(k_{f,z} + A(t) - i\gamma)z} \right. \\ &\quad \left. + \int_{-\infty}^0 dz z \left[e^{i(k_{i,z} - (k_{f,z} + A(t)) - i\kappa)z} + \frac{k_{i,z} - i\gamma}{k_{i,z} + i\gamma} e^{-i(k_{i,z} + (k_{f,z} + A(t)) + i\kappa)z} \right] \right\}. \end{aligned} \quad (3.9)$$

When γ is smallest, for the electrons right at the Fermi energy, $\gamma = \sqrt{2V_0 - k_F^2} = \sqrt{2\phi}$, since $V_0 = \phi + E_F$ and $E_F = k_F^2/2$. This is still about ten times bigger than $\kappa = (2\lambda)^{-1}$. Disregarding the contribution from the positive z -axis, only the two terms from the negative z -axis need to be calculated. These may be done using partial integration, resulting in

$$\langle \psi_{k_f}^V(\vec{r}) | z | \psi_{k_i}(\vec{r}) \rangle = \delta(\vec{k}_{f,\parallel} - \vec{k}_{i,\parallel}) \left[\{\kappa - i(k_{f,z} + A(t) - k_{i,z})\}^{-2} + \frac{k_{i,z} - i\gamma}{k_{i,z} + i\gamma} \{\kappa - i(k_{f,z} + A(t) + k_{i,z})\}^{-2} \right] \quad (3.10)$$

This very simple result is the motivation for choosing the jellium model despite the flaws. When numerical integration is needed to perform the temporal integral in Eq. (2.1), it is required that the spatial integral is analytical and the jellium model satisfies this. In the final state, the free electron state is used in all space, instead of the unbound jellium state. In the limit where the energy of the free electron is large compared to the surface step, V_0 , the solution is of course the free electron, but there energy range considered here is not that far above the surface potential. Since there is only a contribution from within the metal, this is however not important and the only thing that is left is to correct the energy. When the electron reaches the detector, it has passed the surface and the energy the electrons will have in the vacuum is given by $E_v = E - V_0$, where E_v is the electron energy in vacuum and E is the electron energy within the metal. Further, there is a finite probability that an electron excited above the vacuum limit will be reflected from the metal surface and never leave the metal. This is considered later, in Sec. 4.3.

3.1.1 Sidebands in Conduction Band Spectra

When there is a single initial state, the un-assisted ionization spectrum is a single sharp energy peak at $E = \hbar\omega_X - I_p$, where I_p is the ionization potential for the initial state. The laser assisted spectrum is the same central peak and a series of neighbouring peaks, an integer number of photon-energies off the central peak, $E_n = E + n\hbar\omega_L$. When there is not a single initial state, but instead a dense band of initial states as is the case with

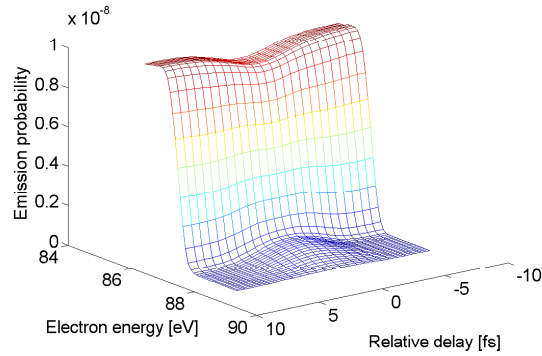


Figure 3.1 | Sidebands from the conduction band are seen as a shoulder to the broad main peak. The shoulder is clearly resolved, even if the duration of the laser pulse is only 3 optical periods and the duration of the xuv pulse is just a single optical period of the laser pulse. The intensity of the assisting laser pulse is $3.2 \cdot 10^{10} \text{ W/cm}^2$.

the conduction band of a metal, the sidebands show up as a shoulder to the peak from the direct transition. This is shown in Fig. 3.1.

In the figure, an 800 nm assisting pulse, with a quite low intensity of $3.2 \cdot 10^{10} \text{ W/cm}^2$ is used. The duration of the xuv pulse is only a single optical period of the assisting laser and the duration of the laser pulse is only three optical periods. When using the sideband as a tool for time-resolved measurements, the temporal resolution is primarily determined by the duration of the laser pulse, and it is interesting to study how the size of the sideband depends on the duration of the laser pulse. This has been plotted in Fig. 3.2.

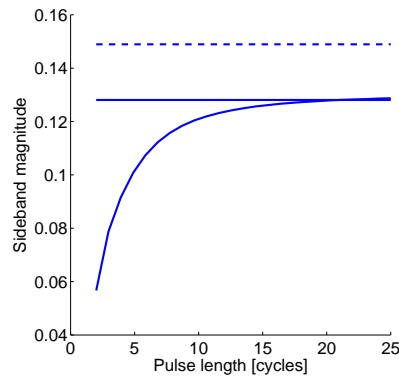


Figure 3.2 | The ratio of the first sideband to the central peak, as a function of laser pulse length. The sideband becomes saturated for a pulse duration longer than 10 optical periods. The two horizontal lines are the atomic result, Eq. (3.11) (full) and the first order Taylor approximation to the same line (dashed). The latter was used in a previous model with an even higher intensity[6].

In the figure is also plotted the value expected from the long pulse limit (where both pulses are long), which is also presented in Eq. (2.15). We see that even though the xuv pulse duration is only a single optical period, the sideband grows to the value expected from the long pulse theory. The first order Taylor expansion is also plotted as the dashed

line

$$P_1 \sim J_1^2 \left(\frac{\vec{k} \cdot \vec{\mathcal{E}}_0}{\omega_L^2} \right) \sim \frac{(\vec{k} \cdot \vec{\mathcal{E}}_0)^2}{4\omega_L^4}. \quad (3.11)$$

In this case, \vec{k} is parallel to $\vec{\mathcal{E}}_0$. The numerator of the fraction is then proportional to the laser intensity and the final energy of the electron. When not performing the Taylor expansion, then the model is seen to be very good for pulses longer than ten optical cycles. In order to achieve very good temporal resolution, pulses shorter than 10 cycles might be preferable, if they are resolvable in the energy spectrum.

3.2 Core Level States

The inner electrons in the atoms do not feel the interaction with the neighbouring atoms, as much as the outer electrons. The electronic state of the outermost electrons are often completely independent on the atomic species and the simple jellium model, completely neglecting the atomic potential for an average potential, may be used to model the conduction band. The inner electrons are much tighter bound to the nucleus, and it is better to use the atomic orbitals as a starting point. Here, we start from a bulk model of the metal, neglecting the surface.

The potential within the metal has a translational symmetry determined by the lattice of the nuclei. The eigenfunctions of a potential with a discrete translational symmetry are known as Bloch waves, and assuming that the core electrons are tightly bound and hence in orbitals resembling the atomic states, the eigenstates are given as

$$\psi_{\text{loc}}^k(\vec{r}) = \frac{1}{\sqrt{N}} \sum_{\vec{R}} e^{i\vec{k} \cdot \vec{R}} \Phi(\vec{r} - \vec{R}), \quad (3.12)$$

where N is the total number of nuclei in the metal, the sum over \vec{R} runs over all the locations of the nuclei and $\Phi(\vec{r})$ is the atomic wavefunction. The energy of this wavefunction is the energy of the atomic state and is independent of the lattice momentum, \vec{k} . The normalization of ψ_{loc} is such that

$$\begin{aligned} \langle \psi_{\text{loc}}^{k'} | \psi_{\text{loc}}^k \rangle &= \frac{1}{N} \sum_{\vec{R}, \vec{R}'} e^{i\vec{k} \cdot \vec{R} - i\vec{k}' \cdot \vec{R}'} \langle \Phi(\vec{r} - \vec{R}') | \Phi(\vec{r} - \vec{R}) \rangle \\ &= \frac{1}{N} \sum_{\vec{R}, \vec{R}'} e^{i\vec{k} \cdot \vec{R} - i\vec{k}' \cdot \vec{R}'} \delta_{\vec{R}, \vec{R}'} = \frac{1}{N} \sum_{\vec{R}} e^{i(\vec{k} - \vec{k}') \cdot \vec{R}} = \sum_{\vec{G}} \delta(\vec{k} - \vec{k}' + \vec{G}). \end{aligned} \quad (3.13)$$

Here, it is assumed that the atomic state is sufficiently tight bound that it does not overlap with the neighbouring orbital and that it is normalized. The δ -function in the end, is in the limit where the metal occupies all space and $N \rightarrow \infty$. The vector \vec{G} is any reciprocal lattice vector, that is, any vector that satisfies that $\vec{R} \cdot \vec{G} = n \cdot 2\pi$ for any lattice vector, \vec{R} . The vector \vec{k} is known as the crystal momentum. It is only conserved up to the reciprocal lattice vector introduced in Eq. (3.13).

Without presenting the detailed form of the atomic wavefunction, it is possible to calculate the dipole matrix element between the Bloch wave and the damped Volkov wave, $\psi_{k_f}^V$, at grazing incidence similar to what was done for the jellium conduction band above. Here $\vec{k}_f(t) = \vec{k}_f + \vec{A}_L(t)$ is introduced to make the notation a bit lighter, such that

$\psi_{k_f}^V = \psi_{k_f(t)}$, where the latter is the free electron wavefunction

$$\begin{aligned} \langle \psi_{k_f}^V | z | \psi_{\text{loc}} \rangle &= \frac{1}{\sqrt{NV}} \int d^3r e^{-i\vec{k}_f(t) \cdot \vec{r}} z e^{\kappa z} \sum_{\vec{R}} e^{i\vec{k}_i \cdot \vec{R}} \Phi(\vec{r} - \vec{R}) \\ &= \frac{\sqrt{v_{\text{cell}}}}{V} \sum_{\vec{R}} e^{i\vec{k}_i \cdot \vec{R}} i \frac{\partial}{\partial k_{f,z}} \int d^3r e^{-i\vec{k}_f(t) \cdot \vec{r}} e^{\kappa z} \Phi(\vec{r} - \vec{R}). \end{aligned} \quad (3.14)$$

Here, v_{cell} is the volume of the Wigner-Seitz cell containing one atom. Since the atomic levels are localized, the integration may be limited to just the Wigner-Seitz cell centered around the atom at \vec{R} instead of the entire half-space. At the same time, if the radius of the Wigner-Seitz cell is small compared to the characteristic damping length, κ , the damping may be taken to be constant over the cell.

$$\begin{aligned} &\sim \frac{i\sqrt{v_{\text{cell}}}}{V} \sum_{\vec{R}} e^{i(\vec{k}_i - \vec{k}_f(t)) \cdot \vec{R}} e^{\kappa R_z} \frac{\partial}{\partial k_{f,z}} \int_{\text{cell}} d^3r e^{-i\vec{k}_f(t) \cdot (\vec{r} - \vec{R})} \Phi(\vec{r} - \vec{R}) \\ &= \frac{i\sqrt{v_{\text{cell}}}}{V} \frac{\partial}{\partial k_{f,z}} \sum_{\vec{R}} e^{i(\vec{k}_i - \vec{k}_f(t)) \cdot \vec{R}} e^{\kappa R_z} \tilde{\Phi}(\vec{k}_f(t)) \\ &= i \frac{(2\pi)^2 \sqrt{v_{\text{cell}}}}{V} \sum_{\vec{G}_{\parallel}} \delta(\vec{k}_{i,\parallel} - \vec{k}_{f,\parallel}(t) + \vec{G}_{\parallel}) \frac{\partial}{\partial k_{f,z}} \frac{\tilde{\Phi}(\vec{k}_f(t))}{1 - \exp(i(k_{i,z} - k_{f,z}(t) + i\kappa)a)}, \end{aligned} \quad (3.15)$$

where a is the lattice constant along the z direction and $\tilde{\Phi}$ is the Fourier transform of the atomic orbital.

To make a simple model of the atomic state, one may model them by hydrogenic states, which are given by

$$\tilde{\Phi}(\vec{k}) = \frac{(2I_p)^{5/4}}{\pi(k^2 + 2I_p)}, \quad (3.16)$$

where I_p is the ionization potential[14].

3.3 Delay of Core Electrons Relative to Conduction Band

As seen in the experiment[5], there is a delay between the core 4f-electrons emitted from a tungsten surface and the conduction band electrons of about 110 asec. The theoretical understanding of the delay is still debated. On one hand, it may be explained by the fact that infrared light incident in the Brewster angle has a short penetration depth, even compared to the short mean free path of the electrons. Then, the finite travel time of the electron wavepackets formed within the metal explains the delay, as the electrons are streaked from the time they reach the surface. This is the idea presented in the experimental paper[5] and this has been supported through one-dimensional, numerical solution of the time dependent Schrödinger equation[15]. Another explanation was first presented in [14]. Here, it is argued that the penetration depth of the infrared field is much longer than the mean free path, and that the relative delay shows up as an interference effect between the different layers of atoms in the metal. This is done in a model similar to the one presented above, for both the conduction band state and the core-level state.

In our model, we may calculate both the streaking spectrum from the conduction band and the core-level state. The parameters used in the calculation are taken from the

experiment. The xuv pulse length is 290 asec (FWHM). The intensity is unknown, but unimportant for the qualitative explanation of the experiment, since it just acts as an overall scaling on the amount of electrons. The infrared laser pulse has a duration of 10 fs. The intensity of the infrared laser pulse is decisive for the amplitude of the streaking, but since the mechanism for the streaking in the metal is not well understood, there is still doubt as to the intensity. Values from $6 \cdot 10^9$ [15] up to $2 \cdot 10^{12}$ [5, 14] W/cm^2 has been used in modelling. Here, the intensity is set to $5 \cdot 10^{10} \text{W}/\text{cm}^2$, for reasons that will be explained when the secondary electrons are included below. For the metal, the Fermi energy is $E_F = 4.5 \text{ eV}$, the workfunction is $\phi = 5.5 \text{ eV}$ and the core, 4f-level is modelled with the hydrogenic s-state of Eq. (3.16), with ionization potential 32.55 eV and a lattice constant, $a = 3.13 \text{ \AA}$. Our model does not have quantitative power and the amount of electrons from the conduction band comes out an order of magnitude lower than the amount from the core levels. To compare, the contribution from the conduction band has been rescaled. The result is shown in Fig. 3.3.

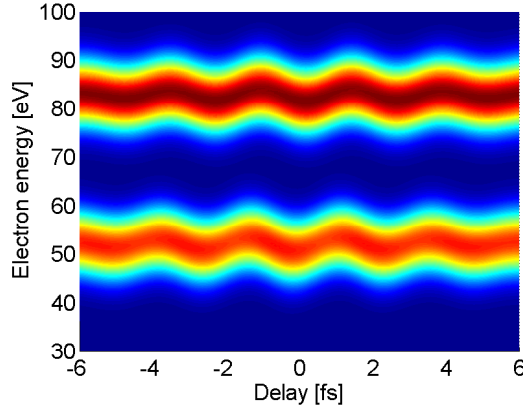


Figure 3.3 | Photoemission spectrum from conduction band electrons and localized 4f-electrons. Parameters are presented in the text. The 4f-electrons are delayed relative to the conduction band electrons, due to interference effects in the metal, but it is difficult to see from the direct spectrum.

The temporal delay between the conduction band and the localized core-state electrons is hard to see from the spectra. To see the delay, a centre-of-energy (CoE) analysis is performed. The centre of energy is defined by

$$E_{\text{CoE}}(t_0) = \frac{\int_{E_{\text{min}}}^{E_{\text{max}}} dE E P(E, t_0)}{\int_{E_{\text{min}}}^{E_{\text{max}}} dE P(E, t_0)} - E_{\text{CoE}}(\infty), \quad (3.17)$$

where $P(E, t_0)$ is the amount of electrons emitted with energy E , when the relative delay between the two laser pulses is t_0 . The last term ensures that when there is no temporal overlap, the CoE is zero. Choosing the limits of the integration such that the CoE corresponding to the conduction band is calculated from $E_{\text{min}} = 67 \text{ eV}$ and the contribution from the 4f-electrons is calculated by integrating up to $E_{\text{max}} = 67 \text{ eV}$, it is possible to find the centre of energy for the conduction band and the core state electrons independently. Plotting $E_{\text{CoE}}(t_0)$ for each of the two parts of the spectra the curves seen in Fig. 3.4. The relative delay between the two curves is 300 asec.

In a very similar model, Ref. [14] reported having seen a shift of 130 asec, similar to the experiment. The difference in the models, is that they had the damping $\kappa = \lambda^{-1}$, instead

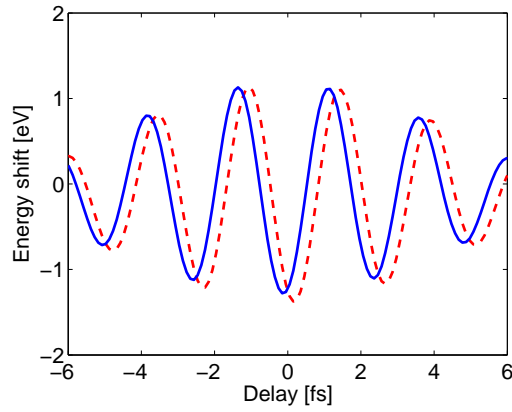


Figure 3.4 | CoE curves for the conduction band electrons (red, dashed) and for the electrons emitted from the 4f-level (blue, full). The delay between the two curves is 300 as, somewhat larger than the experimentally observed delay of 110 as. The CoE from the 4f-electrons has been multiplied by 1.1 in order to make the amplitudes similar.

of $\kappa = (2\lambda)^{-1}$. The delay of the streaking spectra is very sensitive to the damping within the metal. With the choice of κ used here, the norm-square of the electron wavefunction and hence the density of electrons is damped with the characteristic damping parameter λ^{-1} . The reason that our calculation does not fit the experiment may be due to the free electron model. If the electrons are completely free, different layers may interfere to delay the signal from the conduction band electrons and make the relative delay smaller. This remains unresolved.

Secondary Electrons

In the attosecond experiment[5], there is a tail of lower energy electrons, not present in the calculated spectra (compare Figs. 4.6 and 3.3). To describe the tail of low energy electrons following excitation of a metal surface, two different theories are developed. One looks at direct electrons and electrons released after exactly one scattering and another is based on secondary electron cascades. Both theories use a semi-classical approach treating the electrons as located particles propagating within the medium. The amount of electrons released into the vacuum region is then determined by multiplication with the probability of the electron being transmitted through the surface.

The theory is based on the three step model, factoring the photoelectron emission process as i) electron excitation to an unbound state within the metal, ii) electron propagation to the surface and iii) escape through the surface.

4.1 Single-Scattering Theory

First, a theory describing the direct propagation to the surface and propagation with exactly one scattering was developed, based on the work of Berglund and Spicer[16]. We assume that electron propagation within the metal is described by only the inelastic mean free path and that this is shorter than the penetration depth of the exciting pulse. In that case, the amount of electrons, $P(E)$ formed with energy E , per volume is independent of the distance to the surface. The probability for an electron to propagate to the surface without scattering, from a depth $|z|$ within the metal and in an angle θ with the surface normal is given by (see Fig. 4.1)

$$p_{\text{prop}}^0(E, z, \theta) = \exp\left(-\frac{|z|}{\lambda(E) \cos \theta}\right), \quad (4.1)$$

where $\lambda(E)$ is the inelastic mean free path of an electron with energy E .

Integrating this over all depths, z , within the metal, yields the total amount of direct electrons emitted in a direction making the angle θ with the surface normal as

$$N_0(E, \theta) = \int dz p_{\text{prop}}^0(E, z, \theta) P(E) = \lambda(E) P(E) \cos \theta. \quad (4.2)$$

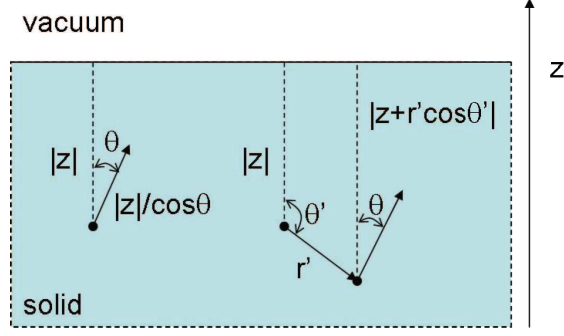


Figure 4.1 | Illustration of emission of a direct(left) and a scattered(right) electron, initially created a distance $|z|$ from the metal surface ($z = 0$).

Most often the direction of interest is along the surface normal, in which case $\cos \theta = 1$. For the scattered electrons, we therefore regard only the electrons ending up along the surface normal.

The amount of electrons reaching the surface along the surface normal after one scattering is given by

$$N_1(E) = \int dz \int dE' p_{\text{prop}}^1(E, E', z) P(E'), \quad (4.3)$$

where $p_{\text{prop}}^1(E, E', z)$, the probability of propagating to the surface from the depth $|z|$, suffering one scattering from the energy E' to the energy E , may be factored as

$$p_{\text{prop}}^1(E, E', z) = \int \frac{d^3 r'}{4\pi\lambda(E')} \exp\left(-\frac{r'}{\lambda(E')}\right) S(E, E') p_{\text{prop}}^0(z + r' \cos \theta', E). \quad (4.4)$$

The first term, $\frac{d^3 r'}{4\pi\lambda(E')} \exp\left(-\frac{r'}{\lambda(E')}\right)$, is the probability of suffering a scattering between r' and $r' + dr'$, the second term, $S(E, E')$ is the probability density for scattering from the energy E' to the energy E , given that a scattering does occur and is assumed to be independent of the angles involved. The third term is the probability that the electron will propagate to the surface without further scatterings, as given by Eq. (4.1). See the right hand side of Fig. 4.1. The integration is over all directions and distances that the electron may travel before suffering the scattering.

Inserting Eq. (4.4) into Eq. (4.3) gives

$$N_1(E) = \int_E^\infty dE' P(E') S(E, E') \int dz \int \frac{d^3 r'}{4\pi\lambda(E')} \exp\left(-\frac{r'}{\lambda(E')}\right) \exp\left(-\frac{|z + r' \cos \theta'|}{\lambda(E)}\right). \quad (4.5)$$

It is assumed that the mean free path is independent of the energy, $\lambda(E') = \lambda(E) = \lambda$, since the universal curve is reasonable flat in the area 20 – 200 eV[13].

The integration over \vec{r}' is bounded by the fact that the scattering must take place within the metal. This integration may be done analytically, by splitting the integral in two, depending on whether the initial direction of the electron is towards or away from

the surface, $\cos \theta' > 0$ or $\cos \theta' < 0$. For $\cos \theta' < 0$, there is no restriction on r'

$$\begin{aligned} & \int \frac{dr'}{4\pi\lambda} \int_{\pi/2}^{\pi} d\theta' 2\pi \sin \theta' \exp\left(-\frac{r'}{\lambda}(1 - \cos \theta')\right) \\ &= \frac{1}{2} \int_{\pi/2}^{\pi} d\theta' \sin \theta' \frac{1}{1 - \cos \theta'} = \log 2/2. \end{aligned} \quad (4.6)$$

For the part where $\cos \theta' > 0$, the r' -integration is restricted to $r' \cos \theta' < -z$, so that the scattering takes place within the metal. This gives

$$\begin{aligned} & \int_0^{\frac{-z}{\lambda \cos \theta'}} \frac{dr'}{4\pi\lambda} \int_{\pi/2}^{\pi} d\theta' 2\pi \sin \theta' \exp\left(-\frac{r'}{\lambda}(1 - \cos \theta')\right) \\ &= \frac{1}{2} \int_{\pi/2}^{\pi} d\theta' \sin \theta' \frac{1 - \exp[-\frac{z}{\lambda}(1 - \sec \theta')]}{1 - \cos \theta'} = \frac{1}{2} \int_0^1 d\xi \frac{1 - \exp[\frac{z\xi}{\lambda(1-\xi)}]}{\xi}, \end{aligned} \quad (4.7)$$

where $\xi = 1 - \cos \theta'$. Now, the z -integral of Eq. (4.3) may be performed

$$\begin{aligned} & \int_{-\infty}^0 dz \left[\frac{\log 2}{2} + \frac{1}{2} \int_0^1 d\xi \frac{1 - \exp[\frac{z\xi}{\lambda(1-\xi)}]}{\xi} \right] e^{z/\lambda} = \frac{\lambda \log 2}{2} + \frac{1}{2} \int_0^1 \frac{\lambda - \lambda \left(1 + \frac{\xi}{1-\xi}\right)^{-1}}{\xi} \\ &= \frac{\lambda \log 2}{2} + \frac{\lambda}{2} \int_0^1 \frac{1 - (1 - \xi)}{\xi} = \lambda \frac{1 + \log 2}{2} \end{aligned} \quad (4.8)$$

Using this result, we find that the total amount of electrons arriving at the surface along the surface normal, unscattered or after one scattering is given as

$$N(E) = N_0(E) + N_1(E) = \lambda P(E) + \lambda \frac{1 + \log 2}{2} \int_E^{\infty} dE' P(E') S(E, E'). \quad (4.9)$$

The only thing left is to find an expression for the scattering probability, S . If it is assumed that the scattering probability is independent of the energies involved. The simplest possible form is to say that the probability for scattering from the energy E' to an energy in the interval $[E, E + dE]$ is given by

$$S^0(E, E') dE = \frac{2dE}{E'}, \quad (4.10)$$

which is to say that all scatterings are equally probable. The factor of 2 is to account for the fact that after each scattering two electrons are present. This scattering may be improved a bit, by including the density of states available for the scattering in a free electron model. In the limit where the energies involved are all much greater than the Fermi energy, E_F , of the metal, we can neglect the energy of the assisting particle. The probability that an electron with energy E' is scattered to the interval $[E, E + dE]$ is then given by

$$S(E, E') dE = \frac{2\rho(E)\rho(E' - E)dE}{\int dE'' \rho(E'')\rho(E' - E'')}. \quad (4.11)$$

The free electron density of states is given by $\rho(E) = \frac{3n}{2E_F} \sqrt{\frac{E}{E_F}}$, where n is the number of conduction band electrons per unit volume. With this approximation, the scattering probability becomes

$$S(E, E') dE = \frac{2\sqrt{E}\sqrt{E' - E}dE}{\int dE'' \sqrt{E''}\sqrt{E' - E''}}. \quad (4.12)$$

Examples of the electron tails following a Gaussian distribution of primary electrons, with the two scattering probabilities given by Eqs. (4.10) and (4.12) are shown in Fig. 4.2

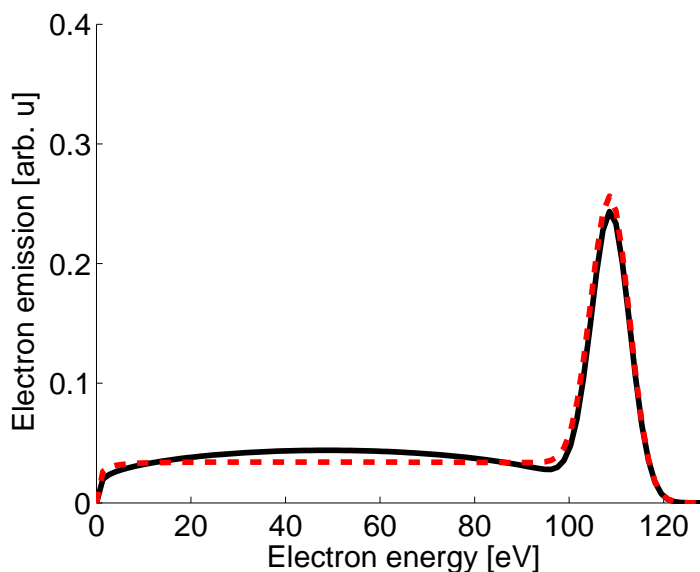


Figure 4.2 | Example of the tail resulting from including a single scattering. The red, dashed curve is made using Eq. (4.10) and the black curve is made using Eq. (4.11).

Neither of these expressions fulfil the Pauli exclusion principle, saying that no scattering can take place that will leave a scattered electron with energy below the Fermi energy, as these states are already occupied. This, however, only changes the shape of the secondary electrons in the region within a few times the Fermi energy of the direct peak and the region below a few times the Fermi energy.

In the energy region that is of interest, it turns out that a single scattering is insufficient. Often, more than one scattering is involved, even when the electron is scattered to energies above 30 eV. A theory involving cascades of secondary electrons is therefore made to account for the plural scatterings. The present theory seems adequate only very close to the direct peak.

4.2 Cascade Theory

Originally, the cascade theory was developed to describe secondary electrons from electron bombardment experiments[17]; a beam of electrons with energy E_0 is directed onto a metal surface along the surface normal. The electrons emitted from the surface are a result of collisions within the metal. Each primary electron has the possibility of colliding inelastically with a conduction band electron, exciting it to an unbound state. Now, each of the unbound electrons has the possibility of knocking another electron free and a cascade of electrons is formed. A very similar process may take place in a photoelectron experiment, using high-energy photons. An electron initially excited by the photon may collide with a number of conduction band electrons before leaving the metal and hence a similar cascade of secondary electrons is formed. In this work, the interest is in the electrons emitted by an attosecond pulse with energies in the xuv, around $\hbar\omega_X = 100$ eV.

The starting point is Boltzmann's transport equation, describing the evolution of the free electrons within the metal

$$\frac{\partial \Phi}{\partial t} + \vec{v} \cdot \nabla \Phi = -\frac{v\Phi}{\lambda} + J + \int dE' \int d\Omega' \frac{v'\Phi'}{\lambda'} S, \quad (4.13)$$

where $\Phi = \Phi(\vec{r}, \vec{\Omega}, E, t)$ is the number of electrons per volume, per energy and per angle, v is the speed of an electron with energy E , J is the source term, the amount of electrons created per volume, energy and angle and S is the scattering probability from energy E' and direction Ω' to E and Ω . From here, a number of approximations are made. First, it is assumed that the electron distribution has azimuthal symmetry. Second, since the penetration depth of the xuv pulse is several nm even at grazing incidence and the inelastic mean free path given by the universal curve is $\lambda \sim 5 \text{ \AA}$ [13], it is assumed that the distribution is independent of the distance to the surface. Finally, it is assumed that the electron-electron scattering is determined by the short range, screened Coulomb interaction. In this case, the electron-electron scattering is nearly isotropic[17]. The Boltzmann equation is then reduced to

$$\frac{v\Phi(E, t)}{\lambda(E)} = J(E, t) + \int dE' \frac{v'\Phi(E', t)}{\lambda(E')} S(E', E) - \frac{\partial \Phi(E, t)}{\partial t}. \quad (4.14)$$

The energy E is the free electron energy within the metal and has $E = 0$ at the bottom of the conduction band.

The fact that the source term, J , is only present for a finite time corresponding to the duration of the exciting pulse, makes it attractive to perform a temporal integration and regard the total amount of electrons arriving at the surface. Recognizing that $v\Phi(E, t)$ is the instantaneous current density through any area parallel to the surface, we find that the amount of electrons arriving at the surface, $N(E)$ satisfies

$$\begin{aligned} \frac{N(E)}{\lambda(E)} &= \int dt J(E, t) + \int dE' \frac{S(E, E')}{\lambda(E')} \int dt v' \Phi(E', t) + \int dt \frac{\partial \Phi(E, t)}{\partial t} \\ &= P(E) + \int dE' \frac{N(E')}{\lambda(E')} S(E, E'), \end{aligned} \quad (4.15)$$

where the last $P(E)$ is the time integral of the source term, the total amount of electrons created at energy E per volume and the last term vanishes since there is no free electrons in the limits long before or after the pulse.

What remains is to find an expression for the scattering term. The simplest possible scattering term is that which is independent of the energy scattered to, E and independent of the angle. This leads to (compare to Eq. (4.10))

$$S(E, E') = \frac{2}{E'}, \quad (4.16)$$

where the factor of 2 ensures that the normalization is such that after each collision, exactly 2 electrons are present. This expression does not fulfil the Pauli exclusion principle, since it allows scattering to electronic states below the Fermi level, which are already occupied. This leads to a correction for the scattering term when the energy E is only a few times the Fermi energy, below the range that we are concerned with (for details, see [17]). One can quite easily give better expressions for this scattering term, but none of these allow for a simple, analytical computation of the distribution of the secondary electrons.

The solution to Eq. (4.15) is given by

$$N(E) = -\lambda(E) \int_E^\infty dE' \left(\frac{E'}{E}\right)^2 \frac{\partial P(E')}{\partial E'} \quad (4.17)$$

which is seen by substitution. $N(E)$ may now be put into a simple form in terms of the source term $P(E)$, by performing integration by parts on Eq. (4.17). This gives the final result for the cascade of electrons inside metal arriving at the surface

$$N(E) = \lambda(E)P(E) + 2\lambda(E) \int_E^\infty dE' \frac{E'}{E^2} P(E'). \quad (4.18)$$

This result is easily interpretable. The first term is the direct part, the amount of electrons created inside the metal that escape to the surface without ever being scattered. The second term represent all the scattered electrons. An electron created with an energy E' gives rise to a cascade of lower energy electrons, determined by the cascade factor, $\frac{2E'}{E^2}$. In the approximations introduced above, the amount and energy distribution of electrons emitted come out as a convolution of the initial spectrum of the formed electrons with a cascade factor. Now the only thing missing is the probability for an electron reaching the surface to actually overcome the surface barrier and escape into the vacuum.

Using this theory, a Gaussian pulse of direct electrons should have a tail of lower energy electrons as shown in Fig. 4.3

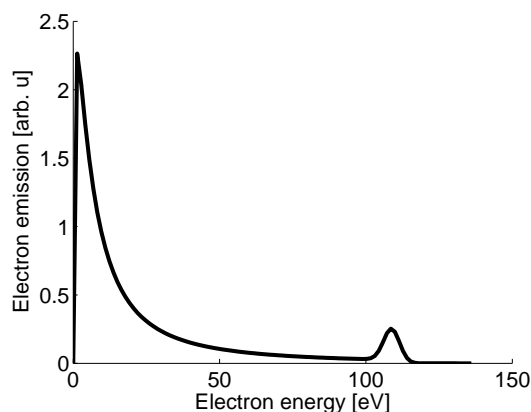


Figure 4.3 | The spectrum of emitted electrons following a Gaussian excitation of 110 eV electrons. The direct electrons are seen as the peak to the right, the rest of the contribution is from the cascade of secondary electrons. This has been multiplied with the transmission probability derived below.

With the assumption that the electron distribution is isotropic within the metal, not only the total amount of electrons passing through a small area of the surface should have this distribution, but also the distribution in each direction on its own. In this way, within the isotropic approximation, the distribution of the electrons coming out of the metal along the surface normal, should be the same. This expression is therefore used to model the distribution along the surface normal.

4.3 Probability for Escaping Through the Surface

The final step missing for describing surface emission is the probability that an electron incident on the surface will escape through the surface. Looking only at the component

along the surface normal, a one dimensional jellium model gives an expression for the transmission probability[18]. The potential is given by the step potential, as in Sec. 3.1

$$V(z) = V_0\Theta(z), \quad (4.19)$$

where $\Theta(z)$ is the Heaviside step function and $V_0 = \phi + E_F$ is the sum of the workfunction and the Fermi energy. For electrons coming from within the metal, with an energy $E > V_0$, the solution takes the form

$$\psi(z) = \Theta(-z) \left[e^{ikz} - A_R e^{-ikz} \right] + \Theta(z) A_T e^{iqz}, \quad (4.20)$$

with A_R and A_T the amplitude for reflection and transmission respectively and $k = \sqrt{2E}$, $q = \sqrt{2(E - V_0)}$. Calculating the current density

$$j = \frac{1}{2i} \left[\psi^* \frac{d\psi}{dz} - \frac{d\psi^*}{dz} \psi \right], \quad (4.21)$$

for both $z < 0$ and $z > 0$ and setting them equal since the number of electrons is conserved gives

$$j = k(1 - |A_R|^2) = q|A_T|^2 \Rightarrow |A_R|^2 + \frac{q}{k}|A_T|^2 = 1. \quad (4.22)$$

Enforcing continuity of both wavefunction and first derivative gives the transmission probability

$$T = \frac{q}{k}|A_T|^2 = \frac{4qk}{(q+k)^2} = \frac{4\sqrt{1 - \frac{V_0}{E}}}{\left(1 + \sqrt{1 - \frac{V_0}{E}}\right)^2}. \quad (4.23)$$

The transmission probability for $V_0 = 10$ eV is plotted in Fig. 4.4.

In the limit $E \rightarrow V_0$ the transmission probability vanishes as the energy approaches the limit where the electron is bound. In the opposite limit, $E \rightarrow \infty$, the transmission probability rapidly approaches unity, as $E > 2V_0$.

For the angular integrated scattering, another expression is used, with $T(E) = 1 - \sqrt{\frac{\phi + E_F}{E}}$, corresponding to the amount of electrons carrying a momentum orthogonal to the surface, great enough to overcome the barrier and escape from the metal. This expression gives a much lower amount of emitted electrons and especially shifts the electrons to higher energies.

The total amount of electrons reaching the vacuum may now be found as the product of the amount reaching the surface and the probability of being transmitted through the surface. This gives a spectrum, when detected in the vacuum region given as $N(E)T(E)$.

4.4 Application to Tungsten Experiment

The previous sections, the tail of the electron distribution is found as a convolution of the direct spectrum with a function describing the scattering, as in Eq. (4.18). If we assume that the initial distribution of the electrons is given as calculated by the T -matrix formalism as described in the previous chapter, then the amount of electrons emitted, both direct and secondaries may be found. Including these secondaries in the electron distribution in Fig. 3.3, results in the electron distribution in Fig. 4.5.

To get a quantitative comparison between the calculated and the measured electron spectrum, a vertical intersection when there is no temporal overlap (corresponding to the

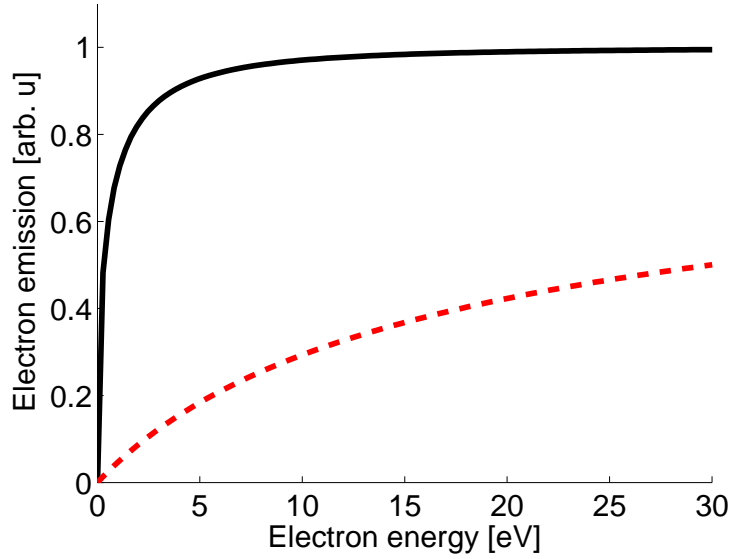


Figure 4.4 | The transmission probability for $\phi + E_F = 10$ eV. The energy scale is relative to the vacuum limit. The transmission probability is for the normal component (Black, full) and for the angular integrated emission (red, dashed).

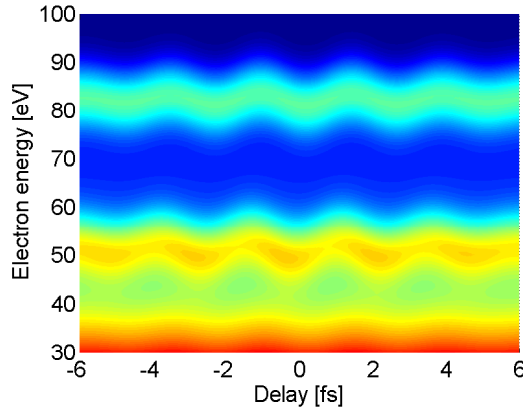


Figure 4.5 | Same figure as Fig. 3.3, but with the inclusion of secondary electrons through Eq. (4.18). The figure is to be compared to the experimental data presented in Fig. 2.2.

dashed, white line in Fig. 2.2) has been made in Fig. 4.6. The size of the tail of secondary electrons is comparable, when the cascade calculation is compared to the experiment. The positions of the peaks are a bit off, due to space-charge effects: At lower energies, a lot of above-threshold electrons are formed. The Coulomb interaction with these electrons pushes the faster high-energy electrons to even higher energies while the low energy-electrons are pushed to lower energies. This is the reason why the experimental 4f-electron peak is shifted up about 3 eV above the theoretical peak. The reason that the conduction band peak is not shifted by the same 3 eV is that our jellium model places the peak about the same 3 eV too high[12]. The problem in the model is that the jellium peak fits, not

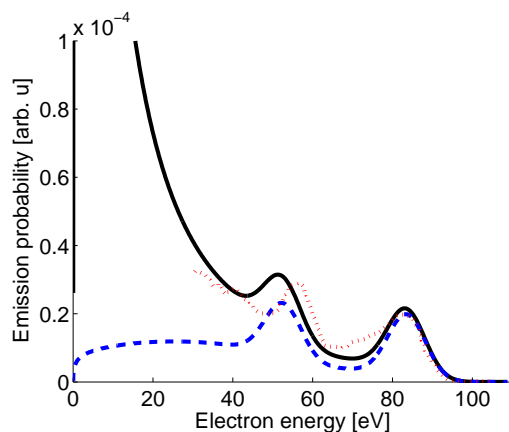


Figure 4.6 | Comparison of the experimental photoelectron spectrum (dotted, red), with the spectrum calculated including only a single scattering (dashed, blue) and using the cascade theory (full, black). The size of the direct peak has been rescaled to allow comparison of the tail of the electrons.

that the 4f-electron peak is off!

When performing the centre-of-energy analysis (Eq. (3.17)), the amplitude of the CoE oscillations is quite sensitive to the size of the background of electrons. When the CoE is calculated from the photoelectron spectrum including the secondary electrons, the amplitude is about half of what it was when the secondaries were not included. Using an intensity of $5 \cdot 10^{10} \text{W/cm}^2$ and including the secondary electrons, the CoE curves are plotted with the experimental data[5] in Fig. 4.7. The signal from the 4f-electrons has been multiplied by a factor of 1.8, where it was multiplied by a factor of 2.5 in the experiment. This is a signature that our background is quantitatively too small, and a sign that the actual intensity is even higher than the one used here.

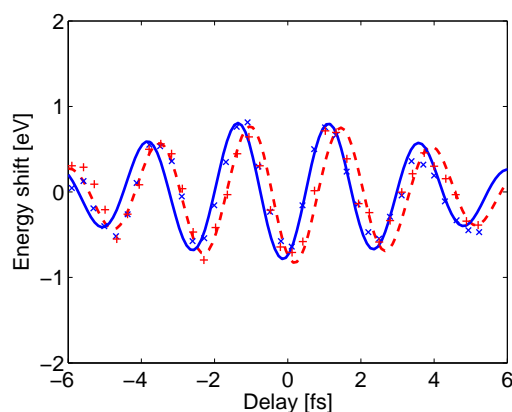


Figure 4.7 | Centre-of-Energy calculated for the 4f-electrons (full, blue) and for the conduction band electrons (red, dashed). The amplitude of the CoE is very dependent on the size of the background. The 4f electron signal has been multiplied by 1.8, whereas the experimental 4f signal was multiplied by 2.5.

When the intensity was calculated in Ref. [15], the calculation seems to have been done based on comparison between the experimental CoE-spectra and a calculated spectrum

without any secondary electrons. This would explain the rather low value of $6 \cdot 10^9 \text{ W/cm}^2$ they find for the intensity of the assisting pulse.

In our theory as presented here, the electron streaking happens as the electrons are formed, in the T -matrix calculation. This is very convenient, but not the correct picture. Using transport theory as presented above, the electrons should interact with the electric field while they propagate to the detector. This of course makes the transport equation more difficult to solve. It is a point to be explored further.

Conclusions and Outlook

In this report, a discussion of the laser assisted photoelectric effect from metal surfaces has been presented. This is a very new field of interest and a lot of things remain unresolved. From an atomic point of view, a model for the laser assisted photoelectron emission is developed. Further, simple theory for the initial states within the metal are presented. A lot of phenomena are explained by these models, like the streaked electron spectra and the sidebands in the limit where the xuv-pulse is longer than the optical period.

One of the things that is not well understood is how the streaking occurs, whether it occurs within the metal[14] or it happens at the surface[15]. This is the same question as to whether the delay observed in the streaking experiment[5] is due to interference between different layers in the solid or due to the finite travel time to the surface of the formed electron wavepackets. One way to shed light on this matter would be to look at the Boltzmann transport equation in an electric field and solve this to see the streaking developing as the electrons propagate. The work on the transport theory has started and has been used to describe the tail of low-energy electrons seen in the spectra, as secondaries, originating from electron-electron scattering within the metal.

All calculations have been made within very simple models of the metal. This is out of necessity, in order to be able to handle the time dependence of the short pulses. In the chapter on the laser assisted photoelectric effect, it is further discussed that a lot of the temporal resolution and the streaking may be explained independently on the detailed form of the metallic states. Yet, it is still important to be able to improve the model, while retaining the computational speed. One way of doing this is to make solid state models based on linear combinations of atomic orbitals, where the atomic orbitals are formed from a Gaussian basis, as is very common in quantum chemistry.

5.1 Transport Theory

In the theory presented in chapter 4, the streaking of the electron spectrum only enters through the initial electron formation, $P(E)$, where it would be more physical, if the streaking occurs as the electron moves in the electric field, after it has been liberated. This may come into the transport equation, Eq. (4.13), by adding the interaction with

the electric field[19]

$$\frac{\partial \Phi}{\partial t} + \vec{v} \cdot \nabla \Phi + \frac{\vec{F}}{m} \cdot \nabla_v \Phi = -\frac{v\Phi}{\lambda} + J + \int dE' \int d\Omega' \frac{v'\Phi'}{\lambda'} S, \quad (5.1)$$

where \vec{F} is the external force and ∇_v is the gradient relative to the velocity. One idea, is to assume the source term, J , to be instantaneous and then propagating the equation. Making similar arguments as in the previous chapter the dimensionality may be reduced sufficiently that this can be done numerically or other approximations may be invoked in order to allow analytical solutions. The main goal would be to reconcile the two differing views as to how the streaking and the delay that is seen in [5] actually comes into a theoretical model.

5.2 Gaussian States

In quantum chemistry, almost all calculations are used in a basis of Gaussian states. With these states, all overlap matrix elements may be calculated analytically, which of course speeds up calculations tremendously. One way of making much better solid state models that still allow analytical calculations of the dipole matrix elements would be to use a basis of spherical Gaussian-type orbitals[20]

$$\phi_{lm}(\alpha, \vec{r}) = N_l(\alpha) e^{-\alpha r^2} \mathcal{Y}_{lm}(\vec{r}), \quad (5.2)$$

where $N_l(\alpha)$ is normalization and $\mathcal{Y}_{lm}(\vec{r})$ is the solid harmonics, related to the usual spherical harmonics through $\mathcal{Y}_{lm} = r^l Y_{lm}(\hat{r})$. Each atomic level that will be a starting point for solid state calculations will be given as linear combinations of ϕ_{lm} functions, with different values of α . This is standard in quantum chemistry and various computational package exists, e.g. GAMESS[21], which is already being used in the group.

When the Hamiltonian has a discrete translational symmetry, $V(\vec{r} + \vec{R}) = V(\vec{r})$ for any lattice vector \vec{R} , the eigenstates may be written as sums of localized states at the atoms

$$\Psi_{n,k}(\vec{r}) = \sum_{\vec{R}} e^{i\vec{k} \cdot \vec{R}} \phi_n(\vec{r} - \vec{R}), \quad (5.3)$$

where the functions ϕ_n are localized states. Using a basis like this, including sufficiently many localized states, the problem of finding the eigenstates corresponding to a particular value of \vec{k} corresponds to solving the matrix equation

$$H_{i,j} \psi = O_{i,j} E \psi, \quad (5.4)$$

where $H_{i,j} = \langle \Psi_i | H | \Psi_j \rangle$ and $O_{i,j} = \langle \Psi_i | \Psi_j \rangle$. If the potential V may be written as a sum of Gaussian potentials around each nucleus, then all the integrations involved in calculating $H_{i,j}$ and $O_{i,j}$ may be calculated analytically. In this way, it is possible to get the initial states as sums of Gaussians, which will allow analytical computation of the dipole matrix elements. This should give much better initial states.

Further, within these Gaussian basis-functions, it is possible to calculate analytically the Auger matrix elements, corresponding to an initial state of two bound electrons and a final state of one bound and one free electron, under the electron-electron Coulomb interaction

$$\langle \phi_{l_a, m_a}(\alpha_a, \vec{r}_1 - \vec{R}_a) e^{i\vec{k} \cdot \vec{r}_2} \Big| \frac{1}{|\vec{r}_1 - \vec{r}_2|} \Big| \phi_{l_b, m_b}(\beta, \vec{r}_1 - \vec{R}_b) \phi_{l_c, m_c}(\gamma, \vec{r}_2 - \vec{R}_c) \rangle. \quad (5.5)$$

This allows the calculation of Auger lifetimes, even when the one-center approximation breaks down. Within such a model, it might be possible to calculate the effect of the surface on the lifetime of an atom adsorbed onto a surface, as it is studied in [6]. Further, it may be possible to calculate Auger lifetimes within a metal surface and in molecules, where the Auger decay is not atomic-like, that is when the two interacting electrons are not centered on the same nucleus, with the hole. The extreme case is a Li_2 molecule following core level ionization, when only the two outer electrons, one from each atom are present.



Bibliography

- [1] J. C. Baggesen and L. B. Madsen, Phys. Rev. A **78**, 032903 (2008).
- [2] J. C. Baggesen and L. B. Madsen, In preparation (2009).
- [3] R. Kienberger, E. Goulielmakis, B. A. Uiberacker, M. and, V. Yakovlev, F. Bammer, A. Scrinzi, T. Westerwalbesloh, U. Kleineberg, U. Heinzmann, M. Drescher, et al., Nature (London) **427**, 817 (2004).
- [4] A. Apolonski, P. Dombi, G. G. Paulus, M. Kakehata, R. Holzwarth, T. Udem, C. Lemell, K. Torizuka, J. Burgdörfer, T. W. Hänsch, et al., Phys. Rev. Lett. **92**, 073902 (2004).
- [5] A. L. Cavalieri, N. Müller, T. Uphues, V. S. Yakovlev, A. Baltuska, B. Horvath, B. Schmidt, L. Blümel, R. Holzwarth, S. Hendel, et al., Nature (London) **449**, 1029 (2007).
- [6] L. Miaja-Avila, G. Saathoff, S. Mathias, J. Yin, C. Laovorakiat, M. Bauer, M. Aeschlimann, M. M. Murnane, and H. C. Kapteyn, Phys. Rev. Lett. **101**, 046101 (2008).
- [7] L. B. Madsen, American Journal of Physics **73**, 57 (2005).
- [8] L. Miaja-Avila, C. Lei, M. Aeschlimann, J. L. Gland, M. M. Murnane, H. C. Kapteyn, and G. Saathoff, Phys. Rev. Lett. **97**, 113604 (2006).
- [9] A. Baltuska, T. Udem, M. Uiberacker, M. Hentschel, E. Goulielmakis, C. Gohle, R. Holzwarth, V. S. Yakovlev, A. Scrinzi, T. W. Hänsch, et al., Nature (London) **421**, 611 (2003).
- [10] E. Goulielmakis, M. Uiberacker, R. Kienberger, A. Baltuska, V. Yakovlev, A. Scrinzi, T. Westerwalbesloh, U. Kleineberg, U. Heinzmann, M. Drescher, et al., Science **305**, 1267 (2004).
- [11] N. W. Ashcroft and N. D. Mermin, *Solid State Physics* (Thomson Learning, 1976).
- [12] N. E. Christensen and B. Feuerbacher, Phys. Rev. B **10**, 2349 (1974).

Bibliography

- [13] A. Zangwill, *Physics at Surfaces* (Cambridge University Press, 1988).
- [14] C.-H. Zhang and U. Thumm, Phys. Rev. Lett. **102**, 123601 (2009).
- [15] A. K. Kazansky and P. M. Echenique, Physical Review Letters **102**, 177401 (2009).
- [16] C. N. Berglund and W. E. Spicer, Phys. Rev. **136**, A1030 (1964).
- [17] P. A. Wolff, Phys. Rev. **95**, 56 (1954).
- [18] E. Merzbacher, *Quantum Mechanics* (Wiley, second edition, 1970).
- [19] F. Reif, *Fundamentals of Statistical and Thermal Physics* (McGraw-Hill, 1985).
- [20] J. Kuang and C. D. Lin, J. Phys. B **30**, 2529 (1997).
- [21] M.W.Schmidt, K.K.Baldrige, J.A.Boatz, S.T.Elbert, M.S.Gordon, J.J.Jensen, S.Koseki, N.Matsunaga, K.A.Nguyen, S.Su, et al., J.Comput.Chem. **14**, 1347 (1993).